2ME2 inhibits tumor growth and angiogenesis by disrupting microtubules and dysregulating HIF

Nicola J. Mabjeesh,[1,3,4] Daniel Escuin,[1,3] Theresa M. LaVallee,[2] Victor S. Pribluda,[2] Glenn M. Swartz,[2] Michelle S. Johnson,[2] Margaret T. Willard,[1] Hua Zhong,[1] Jonathan W. Simons,[1] and Paraskevi Giannakakou[1,*]

[1]Winship Cancer Institute, Emory University School of Medicine, Atlanta, Georgia 30322
[2]EntreMed, Inc., Rockville, Maryland 20850
[3]These authors contributed equally to this work.
[4]Present address: Department of Urology, Tel-Aviv Sourasky Medical Center, Tel-Aviv 64239, Israel.
*Correspondence: paraskevi_giannakakou@emory.org

Summary

Inhibition of angiogenesis is an important new modality for cancer treatment. 2-methoxyestradiol (2ME2) is a novel antitumor and antiangiogenic agent, currently in clinical trials, whose molecular mechanism of action remains unclear. Herein, we report that 2ME2 inhibits tumor growth and angiogenesis at concentrations that efficiently disrupt tumor microtubules (MTs) in vivo. Mechanistically, we found that 2ME2 downregulates hypoxia-inducible factor-1 (HIF) at the posttranscriptional level and inhibits HIF-1-induced transcriptional activation of VEGF expression. Inhibition of HIF-1 occurs downstream of the 2ME2/tubulin interaction, as disruption of interphase MTs is required for HIF-α downregulation. These data establish 2ME2 as a small molecule inhibitor of HIF-1 and provide a mechanistic link between the disruption of the MT cytoskeleton and inhibition of angiogenesis.

Introduction

Angiogenesis, the development of new blood vessels from preexisting vasculature, is essential during embryonic development. In the adult, angiogenesis occurs under physiological conditions in highly regulated processes such as wound healing and ovulation. Under pathological conditions, angiogenesis supports the development of many diseases, including cancer, rheumatoid arthritis, psoriasis, macular degeneration, and diabetic retinopathy (Folkman, 2001). In the case of cancer, angiogenesis is essential for the growth, progression, and metastasis of a tumor and, thus, agents that inhibit angiogenesis are attractive therapeutic options (Hlatky et al., 2002; Weidner et al., 1991). Vascular endothelial growth factor (VEGF) is a major mediator of angiogenesis (Carmeliet et al., 1996; Risau, 1997); whose expression is induced under hypoxic conditions (Goldberg and Schneider, 1994; Minchenko et al., 1994; Shweiki et al., 1992). Induction of VEGF under hypoxic conditions is a multistage process in which the α subunit of hypoxia-inducible factor-1 (HIF-1α) plays a key role (Forsythe et al., 1996). HIF-1α is rapidly degraded by the proteasome under normoxic conditions. This occurs through HIF-1α protein hydroxylation on proline residues 402 and 564 (Ivan et al., 2001; Jaakkola et al., 2001; Masson et al., 2001) by specific HIF-prolyl hydroxylases in the presence of iron and oxygen (Bruick and McKnight, 2001; Epstein et al., 2001). The hydroxylated protein is then recognized by the von Hippel-Lindau tumor suppressor protein (pVHL), which functions as an E3 ubiquitin ligase. The interaction between HIF-1α and pVHL is further accelerated by acetylation of lysine residue 532 through an N-acetyltransferase (Jeong et al., 2002). Under hypoxia, HIF-1α is not hydroxylated, which prevents its interaction with pVHL and its subsequent ubiquitination and degradation. Following hypoxic stabilization, HIF-1α is translocated to the nucleus where it heterodimerizes with HIF-1β (ARNT, arylhydrocarbon receptor nuclear translocator) and activates the transcription of more than 40 genes important for adaptation and survival under hypoxia (Brahimi-Horn et al., 2001; Harris, 2002; Maxwell and Ratcliffe, 2002; Semenza, 2002).

HIF-1α is overexpressed in more than 70% of human cancers and their metastases compared to their adjacent normal tissue, including breast, prostate, brain, lung, and head and neck cancers (Aebersold et al., 2001; Beasley et al., 2002; Birner et al., 2000, 2001; Blancher et al., 2000; Bos et al., 2001; Giatromanolaki et al., 2001; Koukourakis et al., 2002; Schindl et al., 2002; Talks et al., 2000; Zhong et al., 1999). However, the pre-

SIGNIFICANCE

2ME2 is a well-tolerated orally active small molecule with antiangiogenic and antitumor activity currently in phase I/II clinical trials whose exact mechanism of action is not known. Herein, we report on a novel mechanism mediating the antitumor and antiangiogenic activity of 2ME2. Utilizing a pharmacological approach and xenograft models, we showed that at concentrations that are efficacious in vivo, 2ME2 depolymerizes microtubules and blocks HIF-1α nuclear accumulation and HIF-transcriptional activity. This mechanism is shared by other microtubule-targeting drugs used in the clinic. Our data provide evidence for a link between microtubule cytoskeleton disruption, HIF dysregulation, and inhibition of angiogenesis.

cise role of HIF in tumor development remains highly controversial due to the conflicting results of several tumor models. While one study found that genetic disruption of the HIF-1α locus results in the accelerated growth of poorly vascularized HIF-1α$^{-/-}$ teratocarcinomas (Carmeliet et al., 1998), other studies have shown that the absence of HIF activity in different models impairs tumor growth (Hopfl et al., 2002; Maxwell et al., 1997; Ryan et al., 1998, 2000). Additional evidence in support of the notion that HIF is not necessarily a positive regulator of tumor growth emerged from a recent study where ES cells lacking *VHL* and constitutively expressing HIF-α subunits did not promote tumor growth (Mack et al., 2003).

2-Methoxyestradiol (2ME2) is a naturally occurring derivative of estradiol and has been shown to be an orally active, well-tolerated small molecule that possess antitumor and antiangiogenic activity (Pribluda et al., 2000). 2ME2 has low affinity for estrogen receptors α and β, and its antiproliferative activity is independent of the interaction with those receptors (LaVallee et al., 2002). Several mechanisms have been proposed for 2ME2 activity, including those mediated by its ability to bind to the colchicine binding site of tubulin (Cushman et al., 1995; D'Amato et al., 1994) and the inhibition of superoxide dismutase enzymatic activity (Huang et al., 2001). However, some of these findings have been disputed (Attalla et al., 1996; Kachadourian et al., 2001), and the process by which 2ME2 inhibits tumor growth and angiogenesis is still not well understood.

Here we report on a novel mechanism mediating the antitumor and antiangiogenic activity of 2ME2. Our findings demonstrate that 2ME2 destabilizes microtubules at doses that are efficacious in vivo. At concentrations that have antiproliferative activity in tumor cells in vitro, 2ME2 blocks HIF-1α nuclear accumulation and HIF-1 activity by an oxygen- and proteasome-independent pathway. We further show that this mechanism is shared by other MT-targeting drugs, such as taxol, and we provide evidence for a link between the microtubule cytoskeleton and HIF regulation.

Results

2ME2 reduces expression of HIF-1α and VEGF in prostate and breast cancer cells

2ME2 is an effective inhibitor of tumor growth and angiogenesis in numerous in vivo models (Fotsis et al., 1994; Klauber et al., 1997; Pribluda et al., 2000). Although various molecular targets have been proposed for this compound, its mechanism of action remains unclear. HIF-1 is a proangiogenic transcription factor stabilized and activated under hypoxia. HIF-1 activates angiogenesis via transcriptional activation of VEGF, among other genes, and consequently is an important tumor survival factor. In this study, we sought to investigate whether regulation of the HIF-1 pathway could contribute to the antiangiogenic effects of 2ME2. We first examined the effects of 2ME2 treatment on HIF-1α protein in the human prostate cancer cells PC-3 (Figure 1A) and in the human breast cancer cells MDA-MB-231 (Figure 1B). As shown in Figure 1, 2ME2 treatment of PC-3 and MDA-MB-231 cells reduced the levels of nuclear and total HIF-1α protein as detected in nuclear (NE) and whole-cell extract (WCE) preparations. This inhibition was dose dependent and seen under both normoxic and hypoxic conditions. HIF-2α, which has been reported to be regulated similarly to HIF-1α (Semenza, 2000; Wenger, 2000), is also downregulated by 2ME2 (Figure 1B). Treatment with 2ME2 was specific for the regulated α subunit of HIF-1 and HIF-2, but had no effect on the protein levels of HIF-1β or other transcription factors such as c-*fos*, NF-κB (Figure 1A, lower panel), and c-*jun* (data not shown).

To investigate the effects of 2ME2 treatment on HIF-1 transcriptional activity, we measured VEGF protein levels in the conditioned media from 2ME2-treated MDA-MB-231 cells. Consistent with the reduced levels in HIF-1α protein by 2ME2, VEGF levels were also significantly decreased in a dose-dependent manner under both normoxic and hypoxic conditions (Figure 1C). Similar results were obtained following treatment of PC-3 cells with 2ME2 (data not shown).

To examine whether the downregulation of VEGF expression after exposure of cells to 2ME2 was the result of a direct effect on HIF-1α, we tested HIF-1 transcriptional activity using a reporter gene assay (Figure 1D). PC-3 cells were transiently transfected with a construct containing *Luciferase* gene under the control of the hypoxia response elements (HRE) from the *VEGF* promoter (Post and Van Meir, 2001). The results show that 2ME2 treatment also blocked the hypoxia-induced transcriptional activity of HIF-1. To further investigate the effects of 2ME2 treatment on the DNA binding activity of HIF, we performed an electrophoretic mobility shift assay (see Supplemental Figure S1 at http://www.cancercell.org/cgi/content/full/3/4/363/DC1). Consistent with the gene reporter assay (Figure 1D), HIF DNA binding activity was also attenuated in the 2ME2-treated samples. Collectively, these results suggest that 2ME2 inhibits the hypoxia-induced DNA binding and transcriptional activity of HIF.

To determine whether downregulation of HIF-1α by 2ME2 occurred at the transcriptional level, we treated MDA-MB-231 cells with 2ME2 and performed Northern blot analysis (Figure 2A). HIF-1α mRNA levels were not significantly changed by 2ME2 even at very high concentrations (100 μM). Similar results were obtained when we analyzed the expression levels of HIF-1α mRNA with quantitative RT-PCR (data not shown). As expected, hypoxic exposure of the untreated cells resulted in a robust induction (>20-fold) induction in VEGF mRNA (Figure 2A). 2ME2 treatment significantly decreased VEGF mRNA under normoxia (16-fold decrease) and hypoxia (41-fold decrease). It is of note that 2ME2 inhibited VEGF mRNA (Figure 2A) and secretion (Figure 1C) under normoxic conditions as well. This finding is consistent with the inhibition of HIF-1α protein levels by 2ME2 under normoxia. This could be explained by the notion that regulation of VEGF expression in cancer cells with substantial normoxic levels of HIF-1α protein is mediated in part by HIF. In addition, 2ME2 treatment inhibited two other HIF-1 target genes, namely Glut-1 glucose transporter and endothelin-1 (ET-1). This result further confirms that 2ME2 inhibits HIF-1-mediated transcriptional activation of target genes, including VEGF, without affecting the transcription of HIF-1α itself.

To obtain a better understanding of the processes involved in HIF-1α inhibition by 2ME2, we studied the effect of 2ME2 on HIF-1α posttransciptional regulation. We examined 2ME2 effects on HIF-1α protein stability by using the protein translation inhibitor cycloheximide (CHX) (Figure 2B) and a pulse-chase assay (Figure 2C). In the presence of CHX, new protein synthesis is inhibited, thus HIF-1α levels would predominantly reflect the degradation process of HIF-1α protein. Untreated or 2ME2-treated cells were exposed to CHX for various times and HIF-1α protein levels were analyzed by Western blotting. Within 10 min of exposure to CHX (Figure 2B), HIF-1α protein levels from

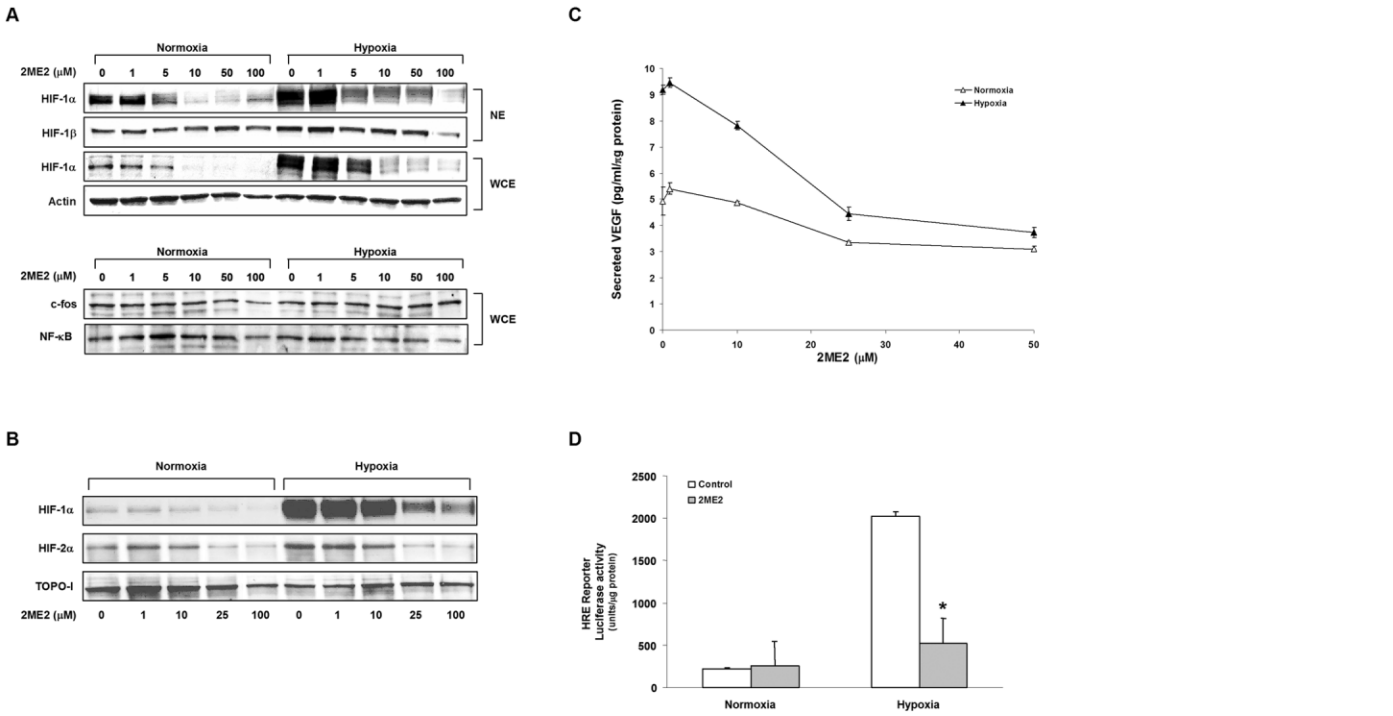

Figure 1. 2ME2 inhibits HIF-1 activity and expression of VEGF in PC-3 and MDA-MB-231 cells

A: PC-3 cells were treated with increasing concentrations of 2ME2 for 16 hr and then subjected to hypoxia, or they remained in normoxia for an additional 6 hr. Nuclear extracts (NE) or whole-cell extracts (WCE) were analyzed by SDS-PAGE and immunoblotted with an antibody against HIF-1α. The blots were stripped and reprobed with HIF-1β, actin, c-Fos, or NF-κB p65.

B: MDA-MB-231 cells were treated with 2ME2 as described in (**A**), and NE were resolved by SDS-PAGE, transferred, and immunoblotted with antibodies against HIF-1α, HIF-2α, and Topoisomerase I (TOPO-I).

C: The conditioned media from MDA-MB-231 cells incubated with 2ME2 were analyzed for VEGF expressed as pg/ml per the total amount of protein in each well.

D: PC-3 cells transiently transfected with pBI-GL V6L were treated with vehicle or 100 μM 2ME2 under normoxic and hypoxic conditions. Relative luciferase activity represents units per μg of protein in each assay point. *Columns*, means; *bars*, SD; n = 3; *, $p < 0.05$.

both untreated and treated cells were decreased to about 60%. Although the intensity of the HIF-1α signal is different at the zero time point, the degradation rates of HIF-1α protein are similar in the absence or the presence of 2ME2 (Figure 2B). This was further confirmed when cells were labeled with ^{35}S-methionine and pulse-chased in the presence or absence of 2ME2, and HIF-1α protein levels were then analyzed. The half-life of HIF-1α from 2ME2-treated cells was approximately 1.5 hr compared to 2.3 hr in the untreated cells. Again, as shown in the graph by the slope of the two curves, the rates of HIF-1α protein loss are similar under both conditions. Thus, 2ME2 does not seem to directly affect HIF-1α protein stability since the rate of decrease of HIF-1α protein from both assays (Figures 2B and 2C) is similar in treated and untreated cells.

Following this observation, we next examined the effect of 2ME2 on HIF-1α protein translation. PC-3 cells were labeled with ^{35}S-methionine in the presence or absence of 2ME2 for the indicated times (min) (Figure 2D). After 15 min of labeling, HIF-1α protein synthesis was at least 10-fold higher in the untreated cells compared with the 2ME2-treated ones (Figure 2D). Together with the results of the protein stability experiments, this result suggests that 2ME2 treatment inhibits HIF-1α protein synthesis rather than enhancing its degradation. To further exclude the possibility that 2ME2 accelerates HIF-1α ubiquitination and degradation through the proteasome, we performed the experiments shown in Figure 2E and Figure S2 (see Supplemental Data on *Cancer Cell* website). PC-3 cells were treated with 2ME2 in the presence or absence of the proteasome inhibitor MG-132 (Figure 2E). In untreated cells, MG-132 resulted as expected in enhanced HIF-1α protein levels and multiple higher molecular weight species, which most likely correspond to poly-ubiquinated HIF-1α protein conjugates (Figure 2E, arrows). In 2ME2-treated cells, however, MG-132 did not restore the inhibitory effect of 2ME2 on HIF-1α protein levels in hypoxia or normoxia, suggesting that 2ME2 does not increase HIF-1α proteasomal-mediated degradation. To further examine whether 2ME2 effects could be attributed to enhanced HIF-1α ubiquitinylation, we transiently transfected cells with FLAG-tagged HIF-1α and examined the accumulation of the ubiquitinated forms of HIF-1α in the presence or absence of 2ME2 (see Supplemental Figure S2 on *Cancer Cell* website). In the presence of 2ME2, there was no change in the amount of ubiquinated HIF-1α compared to control, indicating that 2ME2 affected HIF-1α prior to the ubiquinitation step.

Although, we cannot exclude an indirect effect of 2ME2 on HIF-1α protein degradation through proteasome-independent pathways, our results together with reports on other small molecules (e.g., geldanamycin) known to accelerate HIF-1α protein

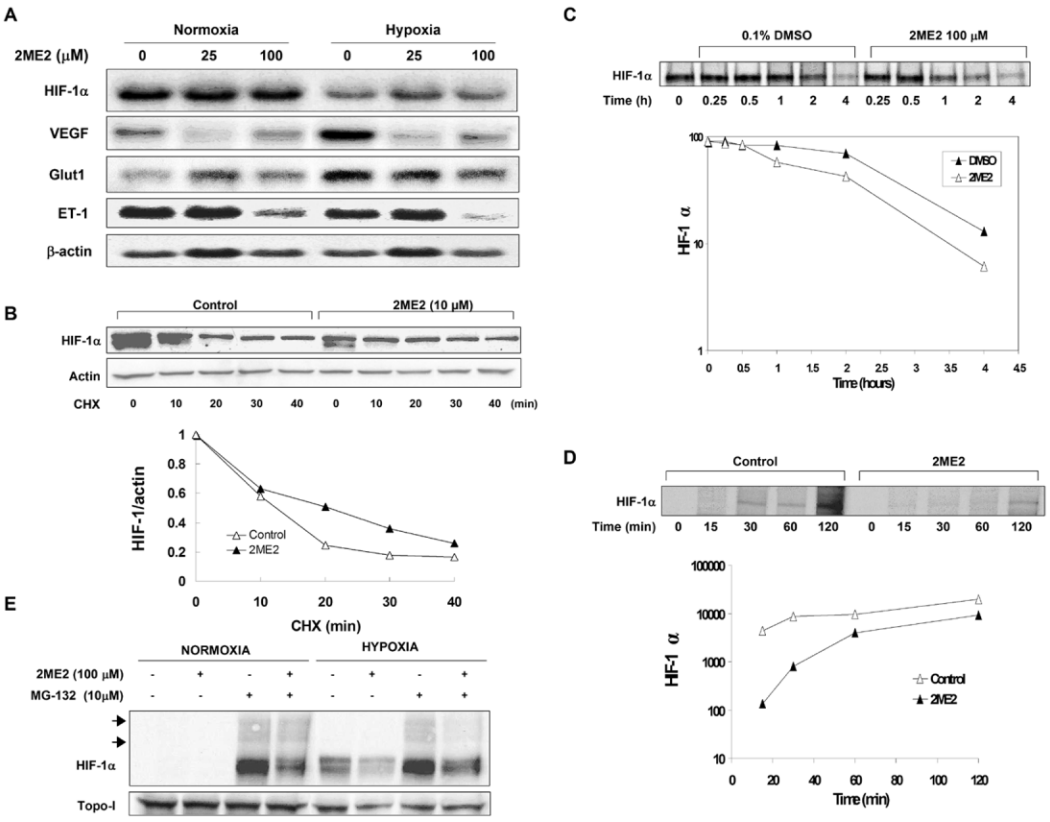

Figure 2. 2ME2 has no effect on HIF-1α mRNA levels or rate of protein degradation

A: Total RNA was prepared from 2ME2-treated MDA-MB-231 cells under normoxic and hypoxic conditions, and Northern blotting was performed with ^{32}P-labeled HIF-1α and $VEGF_{165}$, Glut1, ET-1 probes. β-actin is shown as a loading control. Quantification of the expression levels of VEGF by densitometry was performed using β-actin.

B: *Upper panel*: PC-3 cells were treated overnight with either vehicle (0.01% DMSO) or 10 μM 2ME2 and cycloheximide (CHX) was added at a final concentration of 10 μg/ml for the indicated time. Equal amounts of protein from each sample were resolved by SDS-PAGE, and Western blotting was performed with antibodies against HIF-1α or actin. Lower panel shows quantification of the HIF-1α signal by densitometry following normalization to actin levels. HIF-1α levels from untreated cells or 2ME2-treated cells are arbitrarily given the value of 100%.

C: PC-3 cells were labeled with ^{35}S-methionine and pulse-chased in complete medium containing either 0.1% DMSO or 100 μM 2ME2 for the indicated time (h). *Upper panel*: equal amounts of protein from each cell lysate were subjected to immunoprecipitation with anti-HIF-1α antibody, resolved by SDS-PAGE, and subjected to autoradiography. *Lower panel*: quantification of the autoradiographic HIF-1α signal by densitometry.

D: PC-3 cells were pretreated overnight with either vehicle (0.025% DMSO) or 25 μM 2ME2. The cells were then labeled with ^{35}S-methionine in the presence or absence of 25 μM 2ME2 for the indicated time (min). *Upper panel*: equal amounts of protein from each cell lysate were subjected to immunoprecipitation with anti-HIF-1α antibody, resolved by SDS-PAGE, and subjected to autoradiography. *Lower panel*: quantification of the autoradiographic HIF-1α signal by densitometry.

E: PC-3 cells were treated with 100 μM 2ME2 in the presence and absence of 10 μM MG-132 for 4 hr. Equal amounts of protein from each cell lysate were resolved by SDS-PAGE, transferred, and immunoblotted with antibodies against HIF-1α and TOPO-I. Arrows point to ubiquinated HIF-1α protein species.

ubiquitinylation and proteasomal degradation (Isaacs et al., 2002; Mabjeesh et al., 2002) suggest that 2ME2 reduces HIF-1α protein levels through a translational-dependent pathway rather than affecting HIF-1α protein stability.

2ME2 depolymerizes microtubules and inhibits nuclear accumulation of HIF-1α

2ME2 has been shown to bind to the colchicine binding site of tubulin (D'Amato et al., 1994) and to depolymerize microtubules in endothelial (Fotsis et al., 1994) as well as in tumor cells (Aizu-Yokota et al., 1995), resulting in mitotic arrest and cell death. However, there are also reports demonstrating that the antiproliferative activity of 2ME2 may occur independently of the destabilization of microtubules (Attalla et al., 1996) or by actually stabilizing microtubules (Purohit et al., 1999).

Therefore, we sought to investigate whether there is any correlation between the effects of 2ME2 on microtubules and its effects on HIF-1. We assessed this by laser scanning confocal microscopy (LSCM) in PC-3 cells treated with 2ME2 (Figure 3A). The cells were double-labeled with antibodies against α-tubulin (red) and HIF-1α (green) (Figure 3A). We observed a dose-dependent depolymerization of microtubules in the 2ME2-treated cells (solid arrows) compared to the fine and intricate microtubule network observed in untreated control cells. No significant changes in the microtubule network were observed in untreated cells after hypoxia. On the other hand, while HIF-1α was barely detectable under normoxic conditions, it predominantly accumulated in the nucleus after exposure to hypoxia (Figure 3A, green staining). Nuclear localization of HIF-1α was confirmed by double-labeling with DAPI (data not shown). 2ME2

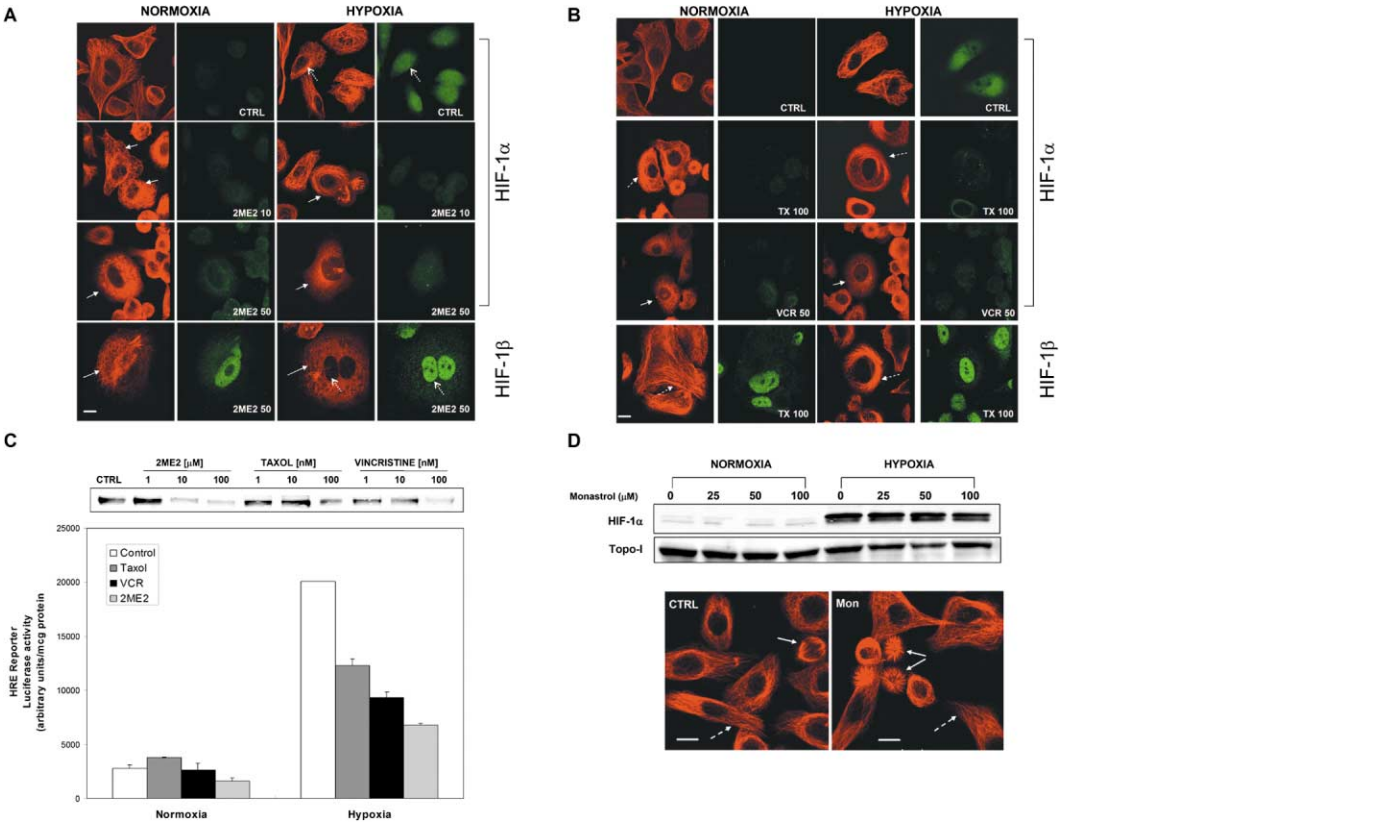

Figure 3. 2ME2 depolymerizes microtubules and impairs nuclear accumulation of HIF-1α

A: PC-3 cells were treated overnight with the indicated concentrations of 2ME2 and then subjected to hypoxia, or they remained in normoxia for an additional 6 hr. Cells were fixed and processed for double immunofluorescence labeling with anti-HIF-1α (green) and anti-α-tubulin (red) antibodies. Staining was analyzed by confocal laser scanning microscopy. As a control, cells were also labeled with antibodies against α-tubulin and HIF-1β (bottom panel). 2ME2 concentration are in μM. Solid arrows point to cells with depolymerized microtubules. Dotted arrows depict nuclear boundaries. Scale bar, 10 μm.

B: A similar experiment was performed with PC-3 cells treated with either taxol (TX) or vincristine (VCR) at the indicated concentrations in nM. Arrows depict cells with depolymerized MTs, dashed arrows depict cells with hyperstabilized MTs forming bundles. Scale bar, 10 μm.

C: PC-3 cells transiently transfected with pBI-GL V6L were treated with vehicle, 2ME2, taxol, or vincristine under normoxic or hypoxic conditions. The cells were then harvested and analyzed for luciferase activity. The upper panel shows a Western blot developed with a HIF-1α antibody of NE of cells treated with indicated drug concentrations under hypoxia.

D: PC-3 cells were treated overnight with either vehicle (0.01% DMSO) or indicated concentrations of Monastrol and processed for Western blotting and confocal microscopy. *Upper panel*: equal amounts of protein from each samples were resolved by SDS-PAGE, and Western blotting was performed with antibodies against HIF-1α or TOPO-I. *Lower panel*: PC-3 cells were fixed and processed for immunofluorescence labeling with anti-α-tubulin (red) antibody. Staining was analyzed by confocal laser scanning microscopy. Solid arrows depict mitotic cells and dotted arrows interphase cells. Notice the difference between a cell normally undergoing mitosis in control cells versus the abnormal monoastral mitotic spindles induced by Monastrol. Also notice that there is difference between interhase microtubules between untreated and treated cells.

treatment significantly reduced the hypoxia-induced nuclear accumulation of HIF-1α. To examine whether these effects were specific for the regulated subunit of HIF-1, HIF-1α, we also tested the effects of 2ME2 on HIF-1β. As seen at the bottom panel of Figure 3A, 2ME2 treatment had no effect on either HIF-1β (green) levels or on HIF-1β subcellular localization. In untreated cells, HIF-1β was localized predominantly in the nucleus, and it was not further accumulated after hypoxia (data not shown).

To determine if the inhibition of HIF-1α was a general property of MT-targeting agents or whether it was specific to 2ME2, we tested other MT-disrupting agents that either destabilize (vincristine) or stabilize (taxol) MTs (Figure 3B). Treatment of PC-3 cells with taxol stabilized MTs, resulting in distinct microtubules bundles (dashed arrows), while vincristine completely depolymerized microtubules (solid arrows) (Figure 3B). Similarly to 2ME2, both taxol and vincristine blocked the hypoxia-induced nuclear accumulation of HIF-1α (Figure 3B) while they had no effect on HIF-1β (Figure 3B and vincristine data not shown). To confirm the data obtained by immunofluorescence and LSCM, we analyzed HIF-1α protein levels and HIF-1 transcriptional activity in cells treated with taxol and vincristine, utilizing 2ME2 as a positive control. Consistent with what was observed with 2ME2 and with their effects on microtubules (Figure 3B), taxol and vincristine also reduced HIF-1α protein levels in a dose-dependent manner (Figure 3C) and inhibited HIF-1 transcriptional activity (Figure 3C).

Since MT-targeting drugs are known to cause mitotic arrest, we wanted to exclude the possibility that the effects of 2ME2, taxol, and vincristine on HIF-1α were nonspecific and reflected rather a "side effect" of mitotic arrest. Thus, we treated MDA-MB231 cells with monastrol, a compound known to induce

mitotic arrest by inhibiting the mitotic kinesin Eg5 but to have no effect on the organization or function of the microtubule cytoskeleton (Mayer et al., 1999). As clearly shown in Figure 3D, monastrol has no effect on HIF-1α protein levels (upper panel) even at concentrations that induce a profound mitotic arrest (lower panel). Consistent with previously published reports on monastrol (Gagescu, 2000) and unlike MT-targeting drugs, we also see no effect on interphase microtubules even at concentrations at which monoastral spindles are observed (Figure 3D, lower panel). Collectively, these results suggest that the strong link between disruption of the microtubule cytoskeleton and inhibition of HIF-1α function is independent of mitotic arrest.

Disruption of the MT cytoskeleton is required for HIF-1α inhibition

The data with these three different classes of MT-targeting drugs indicate that there is good correlation between the disruption of the MT cytoskeleton and the inhibition of HIF-1α. However, the question remains of whether the effects of the MT-targeting drugs on HIF-1α are independent from their effects on the MT cytoskeleton. We addressed this question through a genetic approach employing the 1A9 human ovarian carcinoma cells and its taxol-resistant clone, 1A9/PTX10 (Giannakakou et al., 1997). The 1A9/PTX10 cells are 30-fold resistant to taxol due to an acquired β-tubulin mutation at the taxol binding site, while they retain sensitivity to all MT-depolymerizing agents (Giannakakou et al., 1997) including 2ME2 (data not shown). To assess whether drug-induced effects on microtubules are necessary for inhibition of HIF-1α, we treated the parental 1A9 and the taxol-resistant 1A9/PTX10 cells with taxol and 2ME2 and processed them for LSCM and Western blot analysis (Figure 4). As expected, taxol had no effect on the microtubule network in 1A9/PTX10 cells even at 100 nM, whereas as little as 10 nM of taxol was sufficient to bundle microtubules in the 1A9 parental cells (Figure 4A). In addition, taxol inhibited HIF-1α protein levels in the parental 1A9 cells only, while it had almost no effect on HIF-1α levels in 1A9/PTX10 cells. In contrast, 2ME2 depolymerized MTs and reduced HIF-1α protein levels in both 1A9 and 1A9/PTX10 cells (Figures 4A and 4B). Statistical analysis of three independent experiments (Figure 4C) shows that the ability of taxol and 2ME2 to inhibit HIF-1α levels correlates very well with their ability to affect cellular microtubules. These data extend our previous observations and further suggest that disruption of the normal function of the MT cytoskeleton is required for HIF-1α inhibition by MT-targeting drugs.

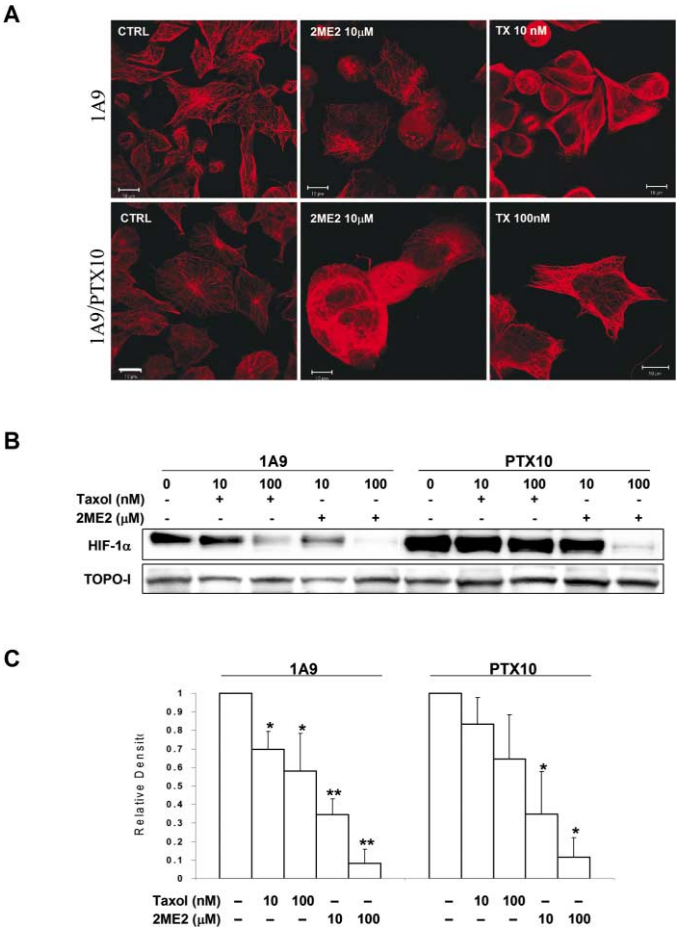

Figure 4. Drug-tubulin interaction is required for inhibition of HIF-1α protein expression

1A9 and PTX10 cells were plated in duplicate, subjected to the indicated treatments overnight followed by hypoxia for an additional 6 hr, and processed for confocal microscopy (**A**) and Western blotting (**B**).

A: Cells were prepared for immunofluorescence staining with an anti-α-tubulin antibody followed by a secondary Alexa 568 antibody. Scale bar, 10 μm.

B: Equal amounts of protein from each cell lysate (NE) were resolved by SDS-PAGE, transferred, and immunoblotted with antibodies against HIF-1α and TOPO-I.

C: Densitometric quantification and statistical analysis of three independent repetitions of the experiment described above. HIF-1α/TOPO-I levels from untreated cells of each experiment were given the value of 1 (100%). Relative densitometry represents arbitrary units of the mean of the three repetitions included in this analysis. *Columns*, means; *bars*, SD; n = 3; * $p < 0.05$; ** $p < 0.01$.

2ME2 inhibits angiogenesis at concentrations that disrupt microtubules in vivo

The concentrations of 2ME2 required to observe the effects on microtubules in vitro are much higher than those achievable in vivo. We employed a mouse orthotopic breast tumor model to determine whether 2ME2 disrupts microtubules at the same doses at which it exhibits antitumor activity in vivo, and to see if this also results in a decrease in the tumor microvascular density. Animals were treated with 2ME2 or cyclophosphamide as a non-MT-targeting chemotherapy drug. At the end of treatment, tumors were excised and processed to assess several different parameters such as tumor volume, vascularization, and integrity of the MT cytoskeleton. As seen in Figure 5A, a dose-dependent reduction of tumor volume was observed with 2ME2 treatment, and at 150 mg/kg, there is a significant reduction in tumor volume when compared to the vehicle-treated control animals (Figure 5A). In addition, time-dependent tumor growth inhibition was also observed in two different animal models of human breast cancer cells (see Supplemental Figure S3 on *Cancer Cell* website). To study the effects of 2ME2 on tumor vascularization, we performed immunohistochemical staining for CD31 in untreated and 2ME2-treated animals, and representative images are shown in Figure 5B. A clear reduction of CD31 staining is seen in the treated animals compared to controls (Figure 5B, upper panel). Statistical analysis of microvessel den-

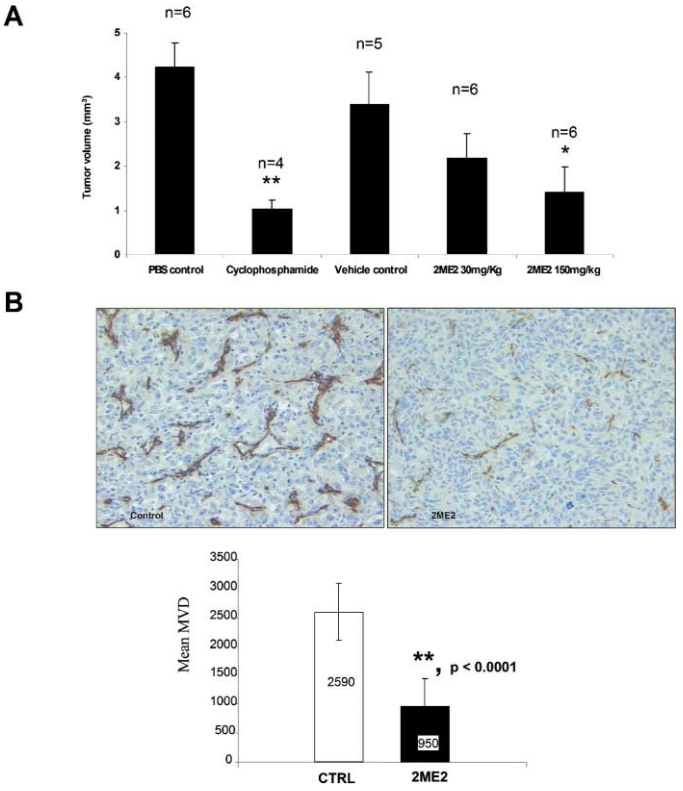

Figure 5. 2ME2 inhibits angiogenesis in a breast cancer orthotopic model

A breast cancer orthotopic model was established using human MDA-MB-231 cells (2×10^6) implanted into the mammary fat pad of female BALB/c nu/nu mice. Animals were treated with the indicated drugs as described in Experimental Procedures, sacrificed after 33 days of treatment, and their tumors were processed for tumor volume measurements (**A**) and CD31 immunohistochemical staining (**B**).

A: Tumor volume measurements were calculated using the formula width^2 $\times$ length $\times$ 0.52. Mean $\pm$ SE of representative experiments is shown. * $p < 0.05$ compared to 1% HPMC vehicle control; ** $p < 0.01$ compared to PBS control.

B: MVD was determined by CD31 immunostaining in 10 paraffin-embedded tumor sections from each animal per cohort. *Upper panel*: a 20$\times$ magnification is shown; 2ME2, 150mg/kg. *Lower panel*: statistical analysis of MVD from all control and 2ME2-treated (150 mg/kg) animals. Columns represent mean MVD and bars represent $\pm$ SEM.

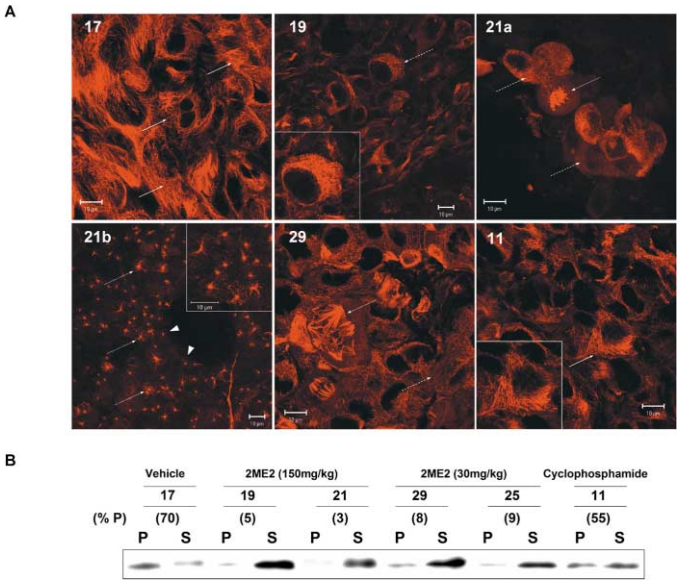

Figure 6. 2ME2 inhibits angiogenesis at concentrations that depolymerize microtubules in vivo

Animals treated with the indicated drugs as described above were sacrificed after 33 days of treatment, and their tumors were processed for tubulin immunofluorescence staining followed by confocal microscopy (**A**) and tubulin Western blotting (**B**).

A: Tubulin immunofluorescence staining with an anti-α-tubulin antibody (red staining) was performed in 50 μm thick tumor sections from treated and untreated animals as indicated. Representative treated animals from each treatment cohort are shown as follows: animal #**17**, vehicle-treated animal; #**19** and #**21**, 2ME2-treated animals at 150 mg/kg; #**29**, 2ME2-treated animal at 30 mg/kg; #**11**, cyclophosphamide-treated animal. Solid arrows depict the fine and intricate microtubule network from untreated animal #**17** or from cyclophosphamide-treated animal #**11** (inset shows higher magnification of one cell from the entire field). Dashed arrows depict cells with depolymerized microtubules from 2ME2- treated (150 mg/kg) animals #**19** and #**21**. Inset in #**19** shows a higher magnification of a cell with profound MT depolymerization. Dotted arrow in #**21a** depicts cells with abnormal mitotic asters as a result of 2ME2 treatment. Dotted arrows in #**21b** (lower magnification) depict cells with aberrant mitotic spindles abnormally arrested in mitosis after 2ME2 treatment. Inset in **#21b** shows a higher magnification of cells with aberrant mitotic spindles. Thick arrowheads point at aberrant mitotic cells lining the vessel. Dashed arrow in #**29** depicts cells with depolymerized MTs and dotted arrow cells with aberrant mitosis after treatment with 30 mg/kg 2ME2. Scale bars, 10 μm.

B: The relative levels of polymerized and soluble tubulin from the tumors of each treated animal were analyzed by Western blotting as described in Experimental Procedures. Lanes P contain the polymerized form of tubulin and lanes S contain the depolymerized soluble form of tubulin. The percentage of polymerized (% P) tubulin from the tumor of each animal was determined by dividing the densitometric value of polymerized tubulin by the total tubulin content.

sity (MVD) from CD31 immunostained tumors was performed by analyzing at least ten sections from each mouse per cohort. This analysis revealed a significant decrease ($p < 0.0001$) in MVD in animals treated with 2ME2 compared to controls (Figure 5B, lower panel).

Then we sought to investigate whether the in vivo effects of 2ME2 on MVD correlated with its antitubulin effects, as we have seen in our experiments with cultured cells. The in vivo effect of 2ME2 on MTs was evaluated by two different assays. First, we developed a highly sensitive method to allow qualitative assessment of the MT cytoskeleton integrity in vivo, using LSCM of tumor sections stained with an antibody against tubulin as described in Experimental Procedures. As shown in Figure 6A, the tumor cells from vehicle or cyclophosphamide-treated mice (animals #17 and #11, respectively) possess a fine, intricate, and well-organized microtubule network (solid arrows). In contrast, the tumor cells from the animals treated with 150 mg/kg 2ME2 (animal #19 and #21a, b) possess either completely depolymerized MTs (dashed arrows) or multiple mitotic asters (dotted arrows), which indicate aberrant mitotic arrest. The latter is more evident in the lower magnification field shown for animal #21 (21b), where almost every cell displayed has aberrant mitotic spindles. The tumor cells from animals treated with 30 mg/kg 2ME2 (animal #29) also have depolymerized MTs (dashed arrows) and multiple aberrant mitotic asters (dotted arrows). This paper reports a qualitative assessment of microtubules in vivo. A section of each tumor excised was processed for Western blot for tubulin analysis in order to assess quantitatively the

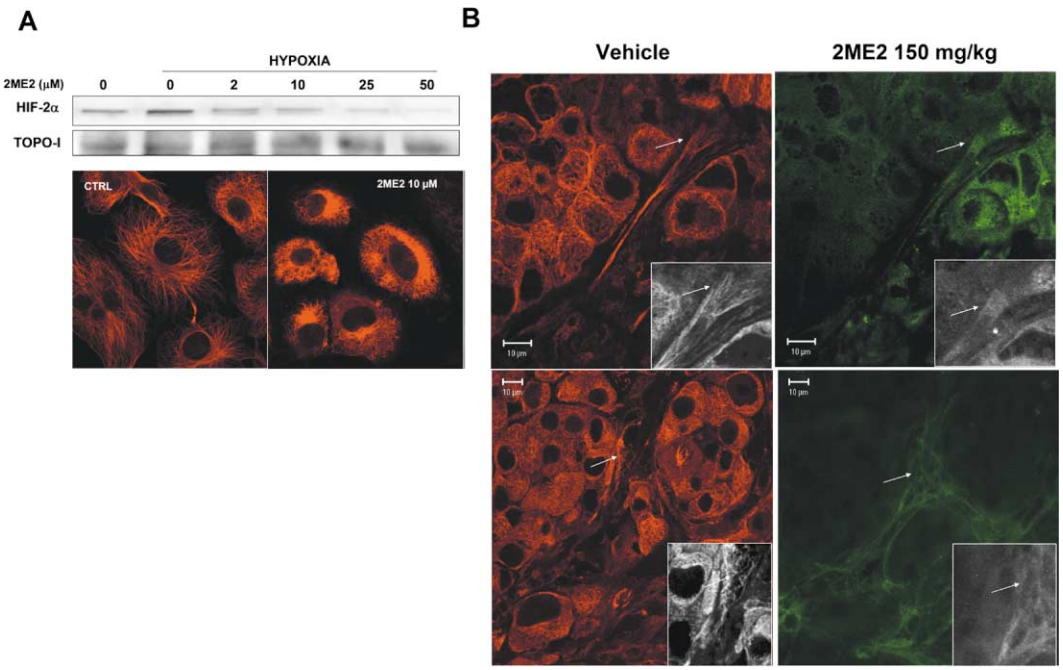

Figure 7. 2ME2 inhibits HIF-2α and depolymerizes microtubules in endothelial cells

A: HUVEC cells were treated with 2ME2 and processed for HIF-2α Western blotting (upper panel) and confocal microscopy for tubulin staining (lower panel). Scale bar, 10 μm.

B: Double labeling immunofluorescence staining with antibodies against α-tubulin (red) and anti-CD31 (green) was performed in tumor sections from treated and untreated animals, as described above. Arrows depict MTs in endothelial cells. Insets show higher magnification of endothelial cell tubulin in gray scale to enhance resolution. Notice the well-organized MT network of endothelial cells in the untreated tumor versus the depolymerized MTs observed in endothelial cells in the 2ME2-treated tumors.

relative levels of polymerized and soluble tubulin following 2ME2 treatment (Figure 6B). In this experiment, we adapted this technique previously developed to assess the effects of MT-targeting drugs on cultured cells (Giannakakou et al., 1997). From each tumor, the lanes labeled "P" contain the polymerized form of tubulin (MTs) and those labeled "S" the soluble form (α/β tubulin dimers). Treatment with 2ME2 depolymerized MTs in a dose-dependent manner. This is evidenced by the decrease from 70% of polymerized tubulin in the vehicle-treated animal to 3%–9% observed in the animals treated with 2ME2. Thus, we have demonstrated by two independent assays that 2ME2 depolymerizes MTs in vivo (Figure 6) at concentrations that inhibit growth and vascularization of tumors (Figure 5).

Careful examination of the in vivo MT staining after 2ME2 treatment suggested that 2ME2 may also have an effect on endothelial cell tubulin, as depicted by the aberrant mitoses seen in cells that line the vessel in animal #21b (Figure 6A, thick arrowheads). This observation prompted us to investigate the effects of 2ME2 on endothelial cells in vitro and in vivo. As shown in Figure 7A and similarly to cancer cells (Figures 1–4), 2ME2 treatment resulted in a dose-dependent inhibition of HIF-2α protein in human umbilical vein endothelial cells (HUVEC) (upper panel), which correlated with extensive microtubule depolymerization (lower panel). Decreased DNA binding activity of HIF measured by EMSA was observed in 2ME2-treated HUVEC cells compared to control untreated cells (data not shown).

We next examined the effects of 2ME2 on endothelial cell tubulin in vivo (Figure 7B). Tumor sections from untreated or 2ME2-treated animals were double-labeled with antibodies against α-tubulin (red staining) and CD31 (green staining). Careful examination of the integrity of MTs in CD31-positive endothelial cells revealed MT disruption in the treated animals compared to the undisturbed MT network in control animals (Figure 7B, insets).

Discussion

Angiogenesis is one of the important biological processes required to support tumor growth beyond a certain threshold size. Therefore, the development of angiogenesis inhibitors has recently become an attractive new strategy to combat cancer. In this study, we have identified a novel molecular mechanism by which 2ME2, an antitumor agent and angiogenesis inhibitor currently in phase I/II trials, exerts its activity. Our results show that 2ME2 depolymerizes MTs and downregulates HIF-1α protein levels and HIF transcriptional activity in an oxygen- and proteasome-independent manner (Figures 1 and 2). Most importantly, we demonstrate that at concentrations that inhibit tumor growth and vascularization in vivo, 2ME2 effectively depolymerizes tumor MTs.

In vitro, 2ME2 has been shown to compete with colchicine for tubulin binding and to disrupt interphase MTs leading to mitotic arrest and cell death in cultured cancer cells (Cushman et al., 1997; D'Amato et al., 1994; Seegers et al., 1997). In addition, when we treated HUVEC with 2ME2, we observed a dose-dependent MT depolymerization at concentrations similar

to those used in tumor cells (Figure 7A). The antiangiogenic properties of this compound, however, had not been correlated previously with its effects on MTs. Other MT-targeting compounds have also been shown to possess varying degrees of antiangiogenic activity, including the colchicine site agents combretastatins (Dark et al., 1997; Grosios et al., 1999; Tozer et al., 2001) and ZD6126 (Blakey et al., 2002) and the taxane site agents, such as taxol, (Belotti et al., 1996; Klauber et al., 1997) docetaxel (Sweeney et al., 2001), and IDN 5390 (Taraboletti et al., 2002). The above studies led to the hypothesis that the antivascular effects of MT-targeting agents derive from their ability to selectively inhibit the growth of endothelial cells in tumor vessels, producing vascular shutdown and massive tumor necrosis. Our data show that 2ME2 affects in vivo tubulin in both the tumor and endothelial cell compartments (Figures 6 and 7), which suggests that 2ME2 may interfere with the crosstalk between cancer and endothelial cells further contributing to the antitumor and antiangiogenic activity of 2ME2.

Decreased VEGF protein levels after 2ME2 treatment have been reported previously (Banerjeei et al., 2000; Chauhan et al., 2002); however, the molecular mechanism responsible for this decrease had not been identified. Our data show that 2ME2 interferes with the downstream activation of HIF-1 target genes, only one of which is VEGF, in response to hypoxia (Figure 2). Thus, our current hypothesis is that the antitumor/antiangiogenic activity of 2ME2 likely results from both the inhibition of the normal function of tumor MTs and the inhibition of the HIF-transcriptome. This hypothesis is supported by data in the literature showing that inhibition of VEGF in vivo by the recombinant humanized antibody directed against VEGF (rhuMAb-VEGF) led to only a 25% inhibition of angiogenesis, whereas 2ME2 inhibited angiogenesis by 63% (Sweeney et al., 2001). This result is in agreement with our in vivo data where a 64% inhibition of angiogenesis was obtained after treatment with 150 mg/kg 2ME2 (Figure 6), and it further suggests that the 2ME2 antiangiogenic activity might not be solely attributed to inhibition of VEGF. Although we attempted to show that 2ME2 inhibited HIF-1 in vivo, we were unable to do so because of the technical challenge in staining HIF-1α in sections form xenograft tumors, unlike our earlier success in staining patients' specimens for HIF-1α from a wide variety of different cancers (Zhong et al., 1999). While we have not been able to confirm all of our in vitro observations in vivo, our data support the hypothesis that 2ME2 affects MTs and its downstream effects on HIF pathway lead to inhibition of tumor vascularization in vivo. We believe further studies using human cancer cells lacking HIF-1 and HIF-2 activity are warranted to conclusively elucidate the important steps involved in this process in vivo.

In our experiments, we have demonstrated that taxol and vincristine also inhibited HIF-1α levels and HIF-1 transcriptional activity (Figure 3). Despite the "opposite" effects of taxol and vincristine on MT structure (stabilization versus destabilization), it is not surprising that both drugs had similar effects on HIF since they both disrupt the organization and equally affect the normal function of the MT cytoskeleton. We further showed that HIF inhibition is not a consequence of mitotic arrest since monastrol, a non-MT-targeting drug that induces mitotic arrest (Mayer et al., 1999), was not able to downregulate HIF-1 levels (Figure 3D). We have also demonstrated that the alterations in the MT cytoskeleton resulting from the interaction of the MT-targeting drugs with tubulin are required for the inhibition of HIF (Figure 4). However we have not yet determined what the signaling events are that link MT disruption to HIF-1α inhibition. Interestingly, a recent study has shown that VHL is a tubulin-associated protein that helps stabilize interphase microtubules, potentially identifying a new role for pVHL function in VHL disease (Hergovich et al., 2003). However, how the pVHL stabilizing effects on MTs may be linked to the VHL-HIF functional regulation is currently unclear (Ratcliffe, 2003). Future studies are warranted to increase our understanding of the molecular mechanisms that regulate these pathways.

Taken together, our results show that disruption of interphase MTs results in repression of HIF-1α, likely at the level of translation, which in turn leads to inhibition of HIF-1 transcriptional activity, including downregulation of VEGF expression. We have further determined that inhibition of HIF-1α by 2ME2 or other MT-targeting compounds occurs downstream of drug-tubulin interaction. This finding provides mechanistic insight into the antiangiogenic mechanism of action reported for several MT-targeting compounds and supports the hypothesis that tubulin-targeting drugs inhibit both tumor cell growth and tumor vascularization following disruption of the MT cytoskeleton. The further characterization of the molecular signals linking the disruption of the MT cytoskeleton with the downregulation of HIF-mediated angiogenesis are likely to identify novel targets for the development of new anticancer therapies.

We believe that pharmacologic inhibition of HIF-1α and particularly HIF-regulated genes that are important for cancer cell survival may be more advantageous than HIF-gene inactivation therapeutic approaches. Conflicting results have emerged from HIF knockout models that showed both accelerated and retarded tumor growth (Carmeliet et al., 1998; Hopfl et al., 2002; Maxwell et al., 1997; Ryan et al., 1998; Ryan et al., 2000), suggesting that genetic inactivation of HIF may not be sufficient to inhibit tumor growth and angiogenesis due to compensatory survival mechanisms acquired by the cancer cells.

2ME2 is currently in phase I/II clinical trials in breast, metastatic breast, and prostate cancer. The preliminary results from these trials show promising responses without any serious drug-related adverse effects even when 2ME2 is administered at doses of 1,000–1,200 mg/day (Lakhani et al., 2003). Herein, we show that 2ME2 is a lead compound that has a dual effect on MTs, a validated anticancer drug target, and HIF, which we believe is an important survival factor in cancer.

Experimental procedures

Chemicals and antibodies

2ME2 was purchased from Tetrionics (Madison, Wisconsin) and 0.1 mM stock solutions were made in DMSO and stored in aliquots at $-80°C$. The compound was diluted in incubation media immediately prior to each experiment. Thawed stock solutions were used once and discarded. Vincristine was from Eli-Lilly (Indianapolis, Indiana), Paclitaxel and Cyclophosphamide were from Sigma (St. Louis, Missouri). MG-132 (Z-Leu–Leu–Leu-aldehyde) was purchased from Alexis Biochemicals (San Diego, California). Monastrol was from AG Scientific, Inc. (San Diego, California). The following primary antibodies were used: rat anti-α-tubulin (Chemicon International, Temecula, California), mouse anti-HIF-1α (BD Biosciences, San Diego, California), rat anti-CD31 (PharMingen, San Diego, California), polyclonal antibody against human HIF-2α and monoclonal HIF-1β (Novus Biologicals, Littleton, Colorado), human actin antibody from Santa Cruz Biotechnology, Inc. (Santa Cruz, California), and polyclonal human antibody to human topoisomerase I (TOPO-I) (TopoGEN, Columbus, Ohio). Rabbit polyclonal antibodies to c-Jun, c-Fos, NF-κB p50, and NF-κB p65 were from Geneka Biotechnology, Inc

(Montréal, Québec, Canada). Secondary antibodies were horseradish peroxidase-conjugated (Amersham Pharmacia Biotech, Piscataway, New Jersey), Alexa Fluor 488 goat anti-mouse (Molecular Probes, Eugene, Oregon), Alexa Fluor 568 goat anti-rat (Molecular Probes, Eugene, Oregon), Rhodamine Red-X mouse anti-rat (Jackson ImmunoResearch, West Grove, Baltimore).

Cell lines

Human breast cancer MDA-MB-231 cells were maintained in DMEM and human prostate cancer PC-3 cells; 1A9 human ovarian carcinoma cells and its paclitaxel-resistant subline 1A9/PTX10 were cultured in RPMI 1640; HUVEC were cultured in M199 media. All media were supplemented with 10% FBS and antibiotics. Cells were cultured at 37°C in a humidified atmosphere and 5% CO_2 in air. For hypoxic exposure, cells were placed in a sealed modular incubator chamber (Billups-Rothenberg, Del Mar, California) flushed with 1% O_2, 5% CO_2, and 94% N_2.

2ME2 treatment of cells

Cells were seeded in culture dishes and grown until 70% confluence. The medium was then replaced with a new medium containing either vehicle (0.1% DMSO) or 2ME2 at the concentrations indicated in the figures for overnight at 37°C. The following day, cells were exposed to hypoxia or left under normoxia for 6 hr. The cells were then washed twice with ice-cold PBS, harvested, and nuclear extract (NE) was prepared as described (Jiang et al., 1996), or alternately, a whole-cell extract (WCE) was prepared by lysing the cells with 100 mM potassium phosphate (pH 7.8) and 0.2% Triton X-100 supplemented with protease and phosphatase inhibitors.

Immunoblot analysis

Proteins (30–60 μg/lane) from WCEs or NEs were resolved by 7.5% SDS-PAGE, electrotransferred to nitrocellulose membrane, and incubated with the indicated primary antibodies, followed by horseradish peroxidase-conjugated secondary antiserum. Immunoreactivity was visualized by enhanced chemiluminescence reagent (Amersham Biosciences, Piscataway, New Jersey). For sequential blotting with additional antibodies, the membranes were stripped using a restore Western blot stripping buffer (Pierce, Rockford, Illinois) and reprobed with the indicated antibodies.

ELISA for VEGF

VEGF concentration in media from treated cells was determined using ELISA kit for VEGF protein (R & D Systems, Inc., Minneapolis, Minnesota) according to the manufacturers' instructions. The results were expressed as concentration of VEGF (pg/ml) per the total protein amount from each well.

Transient transfections and reporter gene assay

PC-3 cells were transfected with 1 μg/well of a reporter plasmid (pBI-GL V6L) containing HREs from the *VEGF* gene as previously described (Mabjeesh et al., 2002; Post and Van Meir, 2001).

Isolation and analysis of RNA

Total RNA was isolated using TRIzol Reagent (Life Technologies, Inc), and Northen blotting was performed with probes specific for human HIF-1α, VEGF 165, endothelin 1 (ET-1), Glut-1 glucose transporter, and β-actin (Ambion, Inc., Austin, Texas) as described (Wang et al., 1995).

HIF-1α protein translation assay

PC-3 cells were plated into 6-well plates and grown to 70% confluence. Cells were pretreated overnight with 25 μM 2ME2 or DMSO (0.025% vol/vol). Then medium was changed to methionine- and cysteine-free as well as serum-free RPMI 1640 medium for 2 hr. After 2 hr, cells were labeled by incubation with methionine- and cysteine-free medium containing ^{35}S-methionine (ICN Biomedicals, Inc., California) at a final concentration of 100 μCi/well at 37°C for the indicated time in the figure. Subsequently, the cells were washed twice with ice-cold PBS, lysed, and subjected for immunoprecipitation using anti-HIF-1α antibody and protein G-agarose beads (Pierce, Illinois) as previously described (Mabjeesh et al., 2002).

Pulse chase assay

PC-3 cells grown in 6-well plates were labeled with ^{35}S-methionine as described above. The radioactive medium was then removed and cells were recultured in complete medium with 0.1% DMSO or 100 μM 2ME2 for various times. Subsequently, the cells were washed twice with ice-cold PBS, lysed, and subjected for immunoprecipitation using anti-HIF-1α antibody as previously described (Mabjeesh et al., 2002).

Tumor models and immunohistochemistry

Female 8- to 10-week-old BALB/c nu/nu mice (Jackson Laboratories, Bar Harbor, Maine) were injected in the mammary fat pad with 2×10^6 MDA-MB-231 cells. Daily oral administration of 2ME2 was initiated when the tumors became palpable (4–5 mm diameter) on day 20 after implantation. A suspension of 2ME2 was prepared by homogenization in an aqueous solution of 0.5% methylcellulose (Sigma) using a Kinematica polytron (Brinkmann, Westbury, New York). At the end of the dosing regimen on day 53 (treatment duration was 33 days), animals were sacrificed and tumor volumes were calculated as width^2 × length × 0.52. Upon termination of the dosing regimen, animals were euthanized with 20 mg/100 g BW of phenobarbital (Sigma), and tumors were excised as quickly as possible and cut into 1 mm^2 pieces. One piece of tumor was dounced and placed into 200 μl of microtubule-stabilizing buffer and processed for the tubulin polymerization assay (for details, see below). The rest of tumor pieces were fixed with 3.7% formaldehyde, 0.05% glutaraldehyde, and 0.5% Triton X-100 in PHEMO buffer for 30 min at room temperature. Then they were transferred into 4% formaldehyde in 0.1 M sodium cacodylate buffer (Sigma) (pH 7.3) for an additional 4 hr. Tumor pieces were stored at 4°C in the same buffer until they were immunostained for α-tubulin, as described above, and CD-31.

Immunohistochemical determination of CD 31/PECAM-1

For immunohistochemistry, tumors were fixed in 10% buffered formalin (Sigma). Paraffin-embedded tissue was sectioned at 5 μm and mounted on Superfrost slides (Fisher Scientific, Co., Houston, Texas). Sections were deparaffinized in xylene, subsequently immersed in graded alcohol (100%, 95% ethanol), rehydrated in ddH_2O and Tris buffer. Sections were then treated with Protinase K (Roche Indianapolis, Indiana), washed in Tris-buffer, blocked for endogenous peroxidase activity by use of 3% hydrogen peroxide in methanol for 20 min. After blocking sections with TNB block for 45 min (NEN Life Science Products, Inc. Boston Massachusetts), sections were incubated with anti-CD31 rat anti-mouse antibody (1:250 dilution) at 4°C overnight (PharMingen, San Diego, California). Slides were then washed TNT wash buffer (NEN), incubated with species-specific biotinylated secondary antibody for 30 min (1:200 dilution, Vector Laboratories, Burlingame, California). After secondary incubation slides were washed in TNT buffer, sections were amplified with tyramide-horderdase peroxidase (NEN) and visualized by incubating the slides with 3, 3′-diaminobenzidine (Vector). The slides were counterstained with Gills Hemotoxylin III (Sigma), rinsed, and immersed briefly in 1% ammonia solution for nuclei binding. Finally, slides were hydrated and mounted with cytoseal (VWR International, West Chester, Pennsylvania) and covered with Fisherfinest glass cover slips (Fisher). For negative controls, the exact procedure was done with either the omission of the primary antibody or the secondary.

Quantification of MVD

For quantification of CD31, tumor sections that stained positive for CD31 vessels were used in the analysis. Microvasular density (MVD) was measured by using Bioquant Image Analysis System (PAI, Frederick, Maryland). To quantify the vessels, ten areas at 168 μm^2 per field at ×200 were captured for each tumor using Olympus BX 40 microscope.

Immunofluorescence and confocal microscopy

A. Cell lines

Exponentially growing cells were plated on 12 mm glass coverslips (Fisher Scientific, Pittsburgh, Pennsylvania) into 24-well plates and cells were allowed to attach overnight. The following day, cells were treated with the indicated drugs for 16 hr and subjected to hypoxia for an additional 6 hr. Cells were fixed with PHEMO buffer (PIPES 0.068M, HEPES 0.025 M, EGTA 0.015 M, $MgCl_2$ 0.003 M, 10% DMSO, pH 6.8) containing 3.7% formaldehyde, 0.05% glutaraldehyde, 0.5% Triton X-100 for 10 min at room temperature. Coverslips were blocked in 10% goat serum/PBS for 10 min and processed for double-labeling immunofluorescence with rat anti-α-tubulin, mouse anti HIF-1α, and mouse anti-HIF-1β antibodies. The secondary antibodies were Alexa Fluor 488 goat anti-mouse antibody and Alexa Fluor 568 goat anti-rat antibody antibodies. Coverslips were then mounted onto glass

slides and examined with a Zeiss axioplasm laser scanning confocal microscope using a Zeiss ×100 1.3 oil-immersion objective.

B. Tumor sections

Animals were treated as described above. For tubulin immunofluorescence followed by LSCM, 1 mm^2 pieces of tumor from each animal were fixed in PHEMO buffer containing 3.7% formaldehyde, 0.05% glutaraldehyde, 0.5% Triton X-100 for 1–2 hr at room temperature. Following fixation, tumor pieces were stored in 4% paraformaldehyde in 0.1% sodium cacodylate at 4°C for up to a month before further processing. Fixed tumor sections were embedded in low-melting agarose (Sigma) and 50 μm sections were obtained by vibratome sectioning at low speed (Vibratome Series 1000 Sectioning System) as previously described (Hale and Matsumoto, 1993). Sections were then processed for α-tubulin immunofluorescence staining and laser scanning confocal microscopy as described above.

Tubulin polymerization assay

The percent of polymerized tubulin from the tumors of the treated animals was assessed as previously described (Giannakakou et al., 1997).

Data analysis

Experiments presented in the figures are representative of three or more different repetitions. Quantification of band densities was performed using the public domain NIH Image (version 1.61). Statistical analysis was performed using a one-way ANOVA test ($p < 0.05$ was considered statistically significant).

Acknowledgments

This work was supported in part by the Avon Foundation with funds raised through the Avon Breast Cancer Crusade, NIH Prostate Cancer SPORE Grant CA-58236, CaP CURE Foundation, and Parisian (N.J.M., H.Z., J.W.S.). N.J.M. is recipient of a fellowship from The American Physicians Fellowship for Medicine in Israel. We wish to thank Dr. Paula Vertino and the Honorable Hamilton Jordan (Winship Cancer Institute, Emory University) for critical discussions and reading of the manuscript and Dr. Dimitris Papanicolaou (Endocrine Division, Emory University School of Medicine) for providing the Glut-1 probe. Finally, we would like to thank Carrie Fredrickson, Cristina Bush, Adam Marcus, Yuefang Wang, and Paula Checchi for technical assistance.

Received: October 29, 2002
Revised: March 12, 2003
Published: April 21, 2003

References

Aebersold, D.M., Burri, P., Beer, K.T., Laissue, J., Djonov, V., Greiner, R.H., and Semenza, G.L. (2001). Expression of hypoxia-inducible factor-1alpha: a novel predictive and prognostic parameter in the radiotherapy of oropharyngeal cancer. Cancer Res. *61*, 2911–2916.

Aizu-Yokota, E., Susaki, A., and Sato, Y. (1995). Natural estrogens induce modulation of microtubules in Chinese hamster V79 cells in culture. Cancer Res. *55*, 1863–1868.

Attalla, H., Makela, T.P., Adlercreutz, H., and Andersson, L.C. (1996). 2-Methoxyestradiol arrests cells in mitosis without depolymerizing tubulin. Biochem. Biophys. Res. Commun. *228*, 467–473.

Banerjeei, S.K., Zoubine, M.N., Sarkar, D.K., Weston, A.P., Shah, J.H., and Campbell, D.R. (2000). 2-Methoxyestradiol blocks estrogen-induced rat pituitary tumor growth and tumor angiogenesis: possible role of vascular endothelial growth factor. Anticancer Res. *20*, 2641–2645.

Beasley, N.J., Leek, R., Alam, M., Turley, H., Cox, G.J., Gatter, K., Millard, P., Fuggle, S., and Harris, A.L. (2002). Hypoxia-inducible factors HIF-1alpha and HIF-2alpha in head and neck cancer: relationship to tumor biology and treatment outcome in surgically resected patients. Cancer Res. *62*, 2493–2497.

Belotti, D., Vergani, V., Drudis, T., Borsotti, P., Pitelli, M.R., Viale, G., Giavazzi, R., and Taraboletti, G. (1996). The microtubule-affecting drug paclitaxel has antiangiogenic activity. Clin. Cancer Res. *2*, 1843–1849.

Birner, P., Schindl, M., Obermair, A., Plank, C., Breitenecker, G., and Oberhuber, G. (2000). Overexpression of hypoxia-inducible factor 1alpha is a marker for an unfavorable prognosis in early-stage invasive cervical cancer. Cancer Res. *60*, 4693–4696.

Birner, P., Schindl, M., Obermair, A., Breitenecker, G., and Oberhuber, G. (2001). Expression of hypoxia-inducible factor 1alpha in epithelial ovarian tumors: its impact on prognosis and on response to chemotherapy. Clin. Cancer Res. *7*, 1661–1668.

Blakey, D.C., Westwood, F.R., Walker, M., Hughes, G.D., Davis, P.D., Ashton, S.E., and Ryan, A.J. (2002). Antitumor activity of the novel vascular targeting agent ZD6126 in a panel of tumor models. Clin. Cancer Res. *8*, 1974–1983.

Blancher, C., Moore, J.W., Talks, K.L., Houlbrook, S., and Harris, A.L. (2000). Relationship of hypoxia-inducible factor (HIF)-1alpha and HIF-2alpha expression to vascular endothelial growth factor induction and hypoxia survival in human breast cancer cell lines. Cancer Res. *60*, 7106–7113.

Bos, R., Zhong, H., Hanrahan, C.F., Mommers, E.C., Semenza, G.L., Pinedo, H.M., Abeloff, M.D., Simons, J.W., van Diest, P.J., and van der Wall, E. (2001). Levels of hypoxia-inducible factor-1 alpha during breast carcinogenesis. J. Natl. Cancer Inst. *93*, 309–314.

Brahimi-Horn, C., Berra, E., and Pouyssegur, J. (2001). Hypoxia: the tumor's gateway to progression along the angiogenic pathway. Trends Cell Biol. *11*, S32–S36.

Bruick, R.K., and McKnight, S.L. (2001). A conserved family of prolyl-4-hydroxylases that modify HIF. Science *294*, 1337–1340.

Carmeliet, P., Dor, Y., Herbert, J.M., Fukumura, D., Brusselmans, K., Dewerchin, M., Neeman, M., Bono, F., Abramovitch, R., Maxwell, P., et al. (1998). Role of HIF-1alpha in hypoxia-mediated apoptosis, cell proliferation and tumour angiogenesis. Nature *394*, 485–490.

Carmeliet, P., Ferreira, V., Breier, G., Pollefeyt, S., Kieckens, L., Gertsenstein, M., Fahrig, M., Vandenhoeck, A., Harpal, K., Eberhardt, C., et al. (1996). Abnormal blood vessel development and lethality in embryos lacking a single VEGF allele. Nature *380*, 435–439.

Chauhan, D., Catley, L., Hideshima, T., Li, G., Leblanc, R., Gupta, D., Sattler, M., Richardson, P., Schlossman, R.L., Podar, K., et al. (2002). 2-Methoxyestradiol overcomes drug resistance in multiple myeloma cells. Blood *100*, 2187–2194.

Cushman, M., He, H.M., Katzenellenbogen, J.A., Lin, C.M., and Hamel, E. (1995). Synthesis, antitubulin and antimitotic activity, and cytotoxicity of analogs of 2-methoxyestradiol, an endogenous mammalian metabolite of estradiol that inhibits tubulin polymerization by binding to the colchicine binding site. J. Med. Chem. *38*, 2041–2049.

Cushman, M., He, H.M., Katzenellenbogen, J.A., Varma, R.K., Hamel, E., Lin, C.M., Ram, S., and Sachdeva, Y.P. (1997). Synthesis of analogs of 2-methoxyestradiol with enhanced inhibitory effects on tubulin polymerization and cancer cell growth. J. Med. Chem. *40*, 2323–2334.

D'Amato, R.J., Lin, C.M., Flynn, E., Folkman, J., and Hamel, E. (1994). 2-Methoxyestradiol, an endogenous mammalian metabolite, inhibits tubulin polymerization by interacting at the colchicine site. Proc. Natl. Acad. Sci. USA *91*, 3964–3968.

Dark, G.G., Hill, S.A., Prise, V.E., Tozer, G.M., Pettit, G.R., and Chaplin, D.J. (1997). Combretastatin A-4, an agent that displays potent and selective toxicity toward tumor vasculature. Cancer Res. *57*, 1829–1834.

Epstein, A.C., Gleadle, J.M., McNeill, L.A., Hewitson, K.S., O'Rourke, J., Mole, D.R., Mukherji, M., Metzen, E., Wilson, M.I., Dhanda, A., et al. (2001). C. elegans EGL-9 and mammalian homologs define a family of dioxygenases that regulate HIF by prolyl hydroxylation. Cell *107*, 43–54.

Folkman, J. (2001). Angiogenesis-dependent diseases. Semin. Oncol. *28*, 536–542.

Forsythe, J.A., Jiang, B.H., Iyer, N.V., Agani, F., Leung, S.W., Koos, R.D., and Semenza, G.L. (1996). Activation of vascular endothelial growth factor gene transcription by hypoxia-inducible factor 1. Mol. Cell. Biol. *16*, 4604–4613.

Fotsis, T., Zhang, Y., Pepper, M.S., Adlercreutz, H., Montesano, R., Nawroth, P.P., and Schweigerer, L. (1994). The endogenous oestrogen metabolite 2-methoxyoestradiol inhibits angiogenesis and suppresses tumour growth. Nature *368*, 237–239.

Gagescu, R. (2000). Another star on drugs. Nat. Rev. Mol. Cell Biol. *1*, 5.

Giannakakou, P., Sackett, D.L., Kang, Y.K., Zhan, Z., Buters, J.T., Fojo, T., and Poruchynsky, M.S. (1997). Paclitaxel-resistant human ovarian cancer cells have mutant beta-tubulins that exhibit impaired paclitaxel-driven polymerization. J. Biol. Chem. *272*, 17118–17125.

Giatromanolaki, A., Koukourakis, M.I., Sivridis, E., Turley, H., Talks, K., Pezzella, F., Gatter, K.C., and Harris, A.L. (2001). Relation of hypoxia inducible factor 1 alpha and 2 alpha in operable non-small cell lung cancer to angiogenic/molecular profile of tumours and survival. Br. J. Cancer *85*, 881–890.

Goldberg, M.A., and Schneider, T.J. (1994). Similarities between the oxygen-sensing mechanisms regulating the expression of vascular endothelial growth factor and erythropoietin. J. Biol. Chem. *269*, 4355–4359.

Grosios, K., Holwell, S.E., McGown, A.T., Pettit, G.R., and Bibby, M.C. (1999). In vivo and in vitro evaluation of combretastatin A-4 and its sodium phosphate prodrug. Br. J. Cancer *81*, 1318–1327.

Hale, I.L., and Matsumoto, B. (1993). Resolution of subcellular detail in thick tissue sections: immunohistochemical preparation and fluorescence confocal microscopy. Methods Cell Biol. *38*, 289–324.

Harris, A.L. (2002). Hypoxia–a key regulatory factor in tumour growth. Nat. Rev. Cancer *2*, 38–47.

Hergovich, A., Lisztwan, J., Barry, R., Ballschmieter, P., and Krek, W. (2003). Regulation of microtubule stability by the von Hippel-Lindau tumour suppressor protein pVHL. Nat. Cell Biol. *5*, 64–70.

Hlatky, L., Hahnfeldt, P., and Folkman, J. (2002). Clinical application of antiangiogenic therapy: microvessel density, what it does and doesn't tell us. J. Natl. Cancer Inst. *94*, 883–893.

Hopfl, G., Wenger, R.H., Ziegler, U., Stallmach, T., Gardelle, O., Achermann, R., Wergin, M., Kaser-Hotz, B., Saunders, H.M., Williams, K.J., et al. (2002). Rescue of hypoxia-inducible factor-1alpha-deficient tumor growth by wild-type cells is independent of vascular endothelial growth factor. Cancer Res. *62*, 2962–2970.

Huang, C.Y., Fujimura, M., Noshita, N., Chang, Y.Y., and Chan, P.H. (2001). SOD1 down-regulates NF-kappaB and c-Myc expression in mice after transient focal cerebral ischemia. J. Cereb. Blood Flow Metab. *21*, 163–173.

Isaacs, J.S., Jung, Y.J., Mimnaugh, E.G., Martinez, A., Cuttitta, F., and Neckers, L.M. (2002). Hsp90 Regulates a von Hippel Lindau-independent Hypoxia-inducible Factor-1alpha-degradative Pathway. J. Biol. Chem. *277*, 29936–29944.

Ivan, M., Kondo, K., Yang, H., Kim, W., Valiando, J., Ohh, M., Salic, A., Asara, J.M., Lane, W.S., and Kaelin, W.G., Jr. (2001). HIFalpha targeted for VHL-mediated destruction by proline hydroxylation: implications for O2 sensing. Science *292*, 464–468.

Jaakkola, P., Mole, D.R., Tian, Y.M., Wilson, M.I., Gielbert, J., Gaskell, S.J., Kriegsheim, A., Hebestreit, H.F., Mukherji, M., Schofield, C.J., et al. (2001). Targeting of HIF-alpha to the von Hippel-Lindau ubiquitylation complex by O2-regulated prolyl hydroxylation. Science *292*, 468–472.

Jeong, J.W., Bae, M.K., Ahn, M.Y., Kim, S.H., Sohn, T.K., Bae, M.H., Yoo, M.A., Song, E.J., Lee, K.J., and Kim, K.W. (2002). Regulation and destabilization of HIF-1alpha by ARD1-mediated acetylation. Cell *111*, 709–720.

Jiang, B.H., Semenza, G.L., Bauer, C., and Marti, H.H. (1996). Hypoxia-inducible factor 1 levels vary exponentially over a physiologically relevant range of O2 tension. Am. J. Physiol. *271*, C1172–C1180.

Kachadourian, R., Liochev, S.I., Cabelli, D.E., Patel, M.N., Fridovich, I., and Day, B.J. (2001). 2-methoxyestradiol does not inhibit superoxide dismutase. Arch. Biochem. Biophys. *392*, 349–353.

Klauber, N., Parangi, S., Flynn, E., Hamel, E., and D'Amato, R.J. (1997). Inhibition of angiogenesis and breast cancer in mice by the microtubule inhibitors 2-methoxyestradiol and taxol. Cancer Res. *57*, 81–86.

Koukourakis, M.I., Giatromanolaki, A., Sivridis, E., Simopoulos, C., Turley, H., Talks, K., Gatter, K.C., and Harris, A.L. (2002). Hypoxia-inducible factor (HIF1A and HIF2A), angiogenesis, and chemoradiotherapy outcome of squamous cell head-and-neck cancer. Int. J. Radiat. Oncol. Biol. Phys. *53*, 1192–1202.

Lakhani, N.J., Sarkar, M.A., Venitz, J., and Figg, W.D. (2003). 2-Methoxyestradiol, a promising anticancer agent. Pharmacotherapy *23*, 165–172.

LaVallee, T.M., Zhan, X.H., Herbstritt, C.J., Kough, E.C., Green, S.J., and Pribluda, V.S. (2002). 2-methoxyestradiol inhibits proliferation and induces apoptosis independently of estrogen receptors alpha and beta. Cancer Res. *62*, 3691–3697.

Mabjeesh, N.J., Post, D.E., Willard, M.T., Kaur, B., Van Meir, E.G., Simons, J.W., and Zhong, H. (2002). Geldanamycin induces degradation of hypoxia-inducible factor 1alpha protein via the proteosome pathway in prostate cancer cells. Cancer Res. *62*, 2478–2482.

Mack, F.A., Rathmell, W.K., Arsham, A.M., Gnarra, J., Keith, B., and Simon, M.C. (2003). Loss of pVHL is sufficient to cause HIF dysregulation in primary cells but does not promote tumor growth. Cancer Cell *3*, 75–88.

Masson, N., Willam, C., Maxwell, P.H., Pugh, C.W., and Ratcliffe, P.J. (2001). Independent function of two destruction domains in hypoxia-inducible factor-alpha chains activated by prolyl hydroxylation. EMBO J. *20*, 5197–5206.

Maxwell, P.H., and Ratcliffe, P.J. (2002). Oxygen sensors and angiogenesis. Semin. Cell Dev. Biol. *13*, 29–37.

Maxwell, P.H., Dachs, G.U., Gleadle, J.M., Nicholls, L.G., Harris, A.L., Stratford, I.J., Hankinson, O., Pugh, C.W., and Ratcliffe, P.J. (1997). Hypoxia-inducible factor-1 modulates gene expression in solid tumors and influences both angiogenesis and tumor growth. Proc. Natl. Acad. Sci. USA *94*, 8104–8109.

Mayer, T.U., Kapoor, T.M., Haggarty, S.J., King, R.W., Schreiber, S.L., and Mitchison, T.J. (1999). Small molecule inhibitor of mitotic spindle bipolarity identified in a phenotype-based screen. Science *286*, 971–974.

Minchenko, A., Bauer, T., Salceda, S., and Caro, J. (1994). Hypoxic stimulation of vascular endothelial growth factor expression in vitro and in vivo. Lab. Invest. *71*, 374–379.

Post, D.E., and Van Meir, E.G. (2001). Generation of bidirectional hypoxia/HIF-responsive expression vectors to target gene expression to hypoxic cells. Gene Ther. *8*, 1801–1807.

Pribluda, V.S., Gubish, E.R., Jr., Lavallee, T.M., Treston, A., Swartz, G.M., and Green, S.J. (2000). 2-Methoxyestradiol: an endogenous antiangiogenic and antiproliferative drug candidate. Cancer Metastasis Rev. *19*, 173–179.

Purohit, A., Singh, A., Ghilchik, M.W., and Reed, M.J. (1999). Inhibition of tumor necrosis factor alpha-stimulated aromatase activity by microtubule-stabilizing agents, paclitaxel and 2-methoxyestradiol. Biochem. Biophys. Res. Commun. *261*, 214–217.

Ratcliffe, P.J. (2003). New insights into an enigmatic tumour suppressor. Nat. Cell Biol. *5*, 7–8.

Risau, W. (1997). Mechanisms of angiogenesis. Nature *386*, 671–674.

Ryan, H.E., Lo, J., and Johnson, R.S. (1998). HIF-1 alpha is required for solid tumor formation and embryonic vascularization. EMBO J. *17*, 3005–3015.

Ryan, H.E., Poloni, M., McNulty, W., Elson, D., Gassmann, M., Arbeit, J.M., and Johnson, R.S. (2000). Hypoxia-inducible factor-1alpha is a positive factor in solid tumor growth. Cancer Res. *60*, 4010–4015.

Schindl, M., Schoppmann, S.F., Samonigg, H., Hausmaninger, H., Kwasny, W., Gnant, M., Jakesz, R., Kubista, E., Birner, P., and Oberhuber, G. (2002). Overexpression of hypoxia-inducible factor 1alpha is associated with an unfavorable prognosis in lymph node-positive breast cancer. Clin. Cancer Res. *8*, 1831–1837.

Seegers, J.C., Lottering, M.L., Grobler, C.J., van Papendorp, D.H., Habbersett, R.C., Shou, Y., and Lehnert, B.E. (1997). The mammalian metabolite, 2-methoxyestradiol, affects P53 levels and apoptosis induction in transformed cells but not in normal cells. J. Steroid Biochem. Mol. Biol. *62*, 253–267.

Semenza, G.L. (2000). HIF-1: mediator of physiological and pathophysiological responses to hypoxia. J. Appl. Physiol. *88*, 1474–1480.

Semenza, G. (2002). Signal transduction to hypoxia-inducible factor 1. Biochem. Pharmacol. *64*, 993–998.

Shweiki, D., Itin, A., Soffer, D., and Keshet, E. (1992). Vascular endothelial growth factor induced by hypoxia may mediate hypoxia-initiated angiogenesis. Nature *359*, 843–845.

Sweeney, C.J., Miller, K.D., Sissons, S.E., Nozaki, S., Heilman, D.K., Shen, J., and Sledge, G.W., Jr. (2001). The antiangiogenic property of docetaxel is synergistic with a recombinant humanized monoclonal antibody against vascular endothelial growth factor or 2-methoxyestradiol but antagonized by endothelial growth factors. Cancer Res. *61*, 3369–3372.

Talks, K.L., Turley, H., Gatter, K.C., Maxwell, P.H., Pugh, C.W., Ratcliffe, P.J., and Harris, A.L. (2000). The expression and distribution of the hypoxia-inducible factors HIF-1alpha and HIF-2alpha in normal human tissues, cancers, and tumor-associated macrophages. Am. J. Pathol. *157*, 411–421.

Taraboletti, G., Micheletti, G., Rieppi, M., Poli, M., Turatto, M., Rossi, C., Borsotti, P., Roccabianca, P., Scanziani, E., Nicoletti, M.I., et al. (2002). Antiangiogenic and antitumor activity of IDN 5390, a new taxane derivative. Clin. Cancer Res. *8*, 1182–1188.

Tozer, G.M., Prise, V.E., Wilson, J., Cemazar, M., Shan, S., Dewhirst, M.W., Barber, P.R., Vojnovic, B., and Chaplin, D.J. (2001). Mechanisms associated with tumor vascular shut-down induced by combretastatin A-4 phosphate: intravital microscopy and measurement of vascular permeability. Cancer Res. *61*, 6413–6422.

Wang, G.L., Jiang, B.H., Rue, E.A., and Semenza, G.L. (1995). Hypoxia-inducible factor 1 is a basic-helix-loop-helix-PAS heterodimer regulated by cellular O2 tension. Proc. Natl. Acad. Sci. USA *92*, 5510–5514.

Weidner, N., Semple, J.P., Welch, W.R., and Folkman, J. (1991). Tumor angiogenesis and metastasis–correlation in invasive breast carcinoma. N. Engl. J. Med. *324*, 1–8.

Wenger, R.H. (2000). Mammalian oxygen sensing, signalling and gene regulation. J. Exp. Biol. *203*, 1253–1263.

Zhong, H., De Marzo, A.M., Laughner, E., Lim, M., Hilton, D.A., Zagzag, D., Buechler, P., Isaacs, W.B., Semenza, G.L., and Simons, J.W. (1999). Overexpression of hypoxia-inducible factor 1alpha in common human cancers and their metastases. Cancer Res. *59*, 5830–5835.